PASJ: Publ. Astron. Soc. Japan , 1–**??**, ⟨publication date⟩

Fundamental Parameters of the Milky Way Galaxy Based on VLBI astrometry

Mareki HONMA,[1,2] Takumi NAGAYAMA,[1] Kazuma ANDO,[3] Takeshi BUSHIMATA,[1] Yoon Kyung CHOI,[4] Toshihiro HANDA,[3] Tomoya HIROTA,[1,2] Hiroshi IMAI,[3] Takaaki JIKE,[1,2] Mi Kyoung KIM,[1] Osamu KAMEYA,[1,2] Noriyuki KAWAGUCHI,[1,2] Hideyuki KOBAYASHI,[1,2,5] Tomoharu KURAYAMA,[3,6] Seisuke KUJI,[1] Naoko MATSUMOTO,[1] Seiji MANABE,[1,2] Takeshi MIYAJI,[1] Kazuhito MOTOGI,[7] Akiharu NAKAGAWA,[3] Hiroyuki NAKANISHI,[3] Kotaro NIINUMA,[1,8] Chung Sik OH,[9] Toshihiro OMODAKA,[3] Tomoaki OYAMA,[1] Nobuyuki SAKAI,[1,2] Katsuhisa SATO,[1] Mayumi SATO,[4] Katsunori M. SHIBATA,[1,2] Satoshi SHIOZAKI,[3] Kazuyoshi SUNADA,[1] Yoshiaki TAMURA,[1,2] Yuji UENO[1] and Aya YAMAUCHI[1]

[1]*Mizusawa VLBI Observatory, NAOJ, Mizusawa, Ohshu, 023-0861*

[2]*Department of Astronomical Science, Graduate University for Advanced Studies, Mitaka, 181-8588*

[3]*Graduate School of Science and Engineering, Kagoshima University, Korimoto, Kagoshima 890-0065*

[4]*Max-Planck-Institute for Radio Astronomy, Auf dem Hügel 69, D-53121, Bonn, Germany*

[5]*Department of Astronomy, The University of Tokyo, Hongo, Bunkyo, Tokyo 113-0033*

[6]*Center for Fundamental Education, Teikyo University of Science, Uenohara, Yamanashi, 409-0193*

[7]*Graduate School of Science, Hokkaido University, N10 W8, Sapporo 060-0810*

[8]*Department of Physics, Yamaguchi University, Yoshida, Yamaguchi, Yamaguchi 753-8512*

[9]*Korean VLBI Network, KASI, Seoul, 120-749, Republic of Korea*

mareki.honma@nao.ac.jp

(Received 2011 October 21; accepted 2012 July 15)

Abstract

We present analyses to determine the fundamental parameters of the Galaxy based on VLBI astrometry of 52 Galactic maser sources obtained with VERA, VLBA and EVN. We model the Galaxy's structure with a set of parameters including the Galaxy center distance R_0, the angular rotation velocity at the LSR Ω_0, mean peculiar motion of the sources with respect to Galactic rotation ($U_{\rm src}$, $V_{\rm src}$, $W_{\rm src}$), rotation-curve shape index, and the V component of the Solar peculiar motions $V_\odot$. Based on a Markov chain Monte Carlo method, we find that the Galaxy center distance is constrained at a 5% level to be $R_0 = 8.05 \pm 0.45$ kpc, where the error bar includes both statistical and systematic errors. We also find that the two components of the source peculiar motion $U_{\rm src}$ and $W_{\rm src}$ are fairly small compared to the Galactic rotation velocity, being $U_{\rm src} = 1.0 \pm 1.5$ km s $^{-1}$ and $W_{\rm src} = -1.4 \pm 1.2$ km s^{-1}. Also, the rotation curve shape is found to be basically flat between Galacto-centric radii of 4 and 13 kpc. On the other hand, we find a linear relation between $V_{\rm src}$ and $V_\odot$ as $V_{\rm src} = V_\odot - 19\,(\pm 2)$ km s^{-1}, suggesting that the value of $V_{\rm src}$ is fully dependent on the adopted value of $V_\odot$. Regarding the rotation speed in the vicinity of the Sun, we also find a strong correlation between Ω_0 and $V_\odot$. We find that the angular velocity of the Sun, $\Omega_\odot$, which is defined as $\Omega_\odot \equiv \Omega_0 + V_\odot / R_0$, can be well constrained with the best estimate of $\Omega_\odot = 31.09 \pm 0.78$ km s^{-1} kpc^{-1}. This corresponds to $\Theta_0 = 238 \pm 14$ km s^{-1} if one adopts the above value of R_0 and recent determination of $V_\odot \sim$12 km s^{-1}.

Key words: astrometry — VLBI — The Galaxy — Galactic parameters

1. Introduction

As a first-order approximation, the Milky Way Galaxy can be regarded as an axi-symmetric system with a circular rotation, and its structure and motions can be described combinations of fundamental parameters. For instance, historically the Milky Way's rotation was discovered based on the determinations of so-called Oort constants A and B, which are combinations of the distance to the Galaxy center R_0, and the rotation velocity of the LSR (Local Standard of Rest) Θ_0, and their derivatives. Today the Galactic constants R_0 and Θ_0 are most frequently-used parameters which provide fundamental scales of the Galaxy's size and rotation speed. The IAU recommendation values are 8.5 kpc and 220 km s^{-1}, (Kerr & Lynden-Bell 1986), but accurate values of these parameters are still at issue: for instance, most of recent studies of R_0 favor values somewhat smaller than the IAU value (Reid 1993: Ghez et al. 2008; Gilssen et al. 2009; McMillan & Binney 2010), being between 8.0 and 8.5 kpc. The rotation curve is another important quantity to describe the rotation and mass distributions in the Galaxy, and often parameterized with a few parameters (e.g., flat rotation curve or power-law rotation curve). However, the exact shape of the rotation curve also remains yet to be studied.

Astrometry of Galactic sources is believed to be most powerful to determine the fundamental parameters of the Galaxy because it provides full six-dimensional phase-space information of Galactic objects. Most notably, until recently most of parallax measurements have been limited to local sources, within $\sim$1 kpc from the Sun (for instance, such as using HIPPARCOS). However, recent development of high-accurate astrometry with VLBI is now providing tens of sources for which precise distances and proper motions are known. Thanks to this, new determination of fundamental parameters of the Milky Way Galaxy becomes feasible. For instance, Reid et

al. (2009b) used 18 maser sources to explore the structure of the Milky Way and obtained the Galactic parameters such as $R_0 = 8.4 \pm 0.6$ kpc and $\Theta_0 = 254 \pm 16$ km s^{-1}. In addition, they suggested that rotation of star-forming regions could lag behind the true Galactic rotation by $\sim$15 km s^{-1}. There are also several studies of Galactic structures based on reanalysis of Reid et al.' data (e.g., Bobylev & Bajkova 2010; McMillan & Binney 2010), which emphasize importance of Galactic scale astrometry. Since VLBI astrometry has been now extensively carried out with VERA and VLBA, the number of sources for which astrometric information is available is significantly increased (e.g., there are $\sim$10 new sources reported in the VERA special issue in PASJ 63, 2011). Therefore, it is worth conducting a new study of fundamental parameters of the Galaxy based on these new results. To carry out this, in this paper we compile the most-updated list of VLBI astrometry results, and provide new analyses of fundamental parameters of the Milky Way Galaxy.

2. Sample

We collected results of VLBI astrometry from the literatures including most recent results, and compiled a list of parallaxes and proper motions in table 1. The list consists of star-forming regions with maser sources or continuum sources (such as T-Tau stars) that have been observed with VERA (VLBI Exploration of Radio Astrometry)/VLBA (Very Long Baseline Array)/EVN (European VLBI Network). The star-forming regions included here are those with H_2O and/or CH_3OH maser emissions, or gyro-synchrotron emissions which originate from magnetic activity of pre-main sequence stars. We include in our sample almost all published works available to date: the only exceptions are: 1) Sgr B2 (Reid et al.2009c), which is too close to the Galaxy center (expected to be at $\sim$100 pc) and is known to have significant peculiar motion, making this sources unsuitable for the study of the Galactic rotation, 2) G34.43+0.24 (Kurayama et al. 2011) for which the proper motion in declination is not measured due to poor UV coverage for this nearly-0 declination source, and 3) IRAS 05137+3919 (Honma et al. 2011), which is likely to be located in the far outer Galaxy ($R \geq 15$ kpc), where our simple parameterization of Galactic rotation (e.g., power-low rotation curve) may not be appropriate.

We only selected star-forming regions, and excluded late-type stars because properties of these populations are quite different from those of star-forming regions: for instance, late-type stars are known to have a larger velocity dispersion than that of star-forming regions, and their rotation lags behind the Galactic rotation, which is known as "asymmetric drift". However, we note that we included two super-giant sources VY CMa (Choi et al. 2008) and S Per (Asaki et al. 2010) since they are massive stars that evolve quickly after their birth, and thus can be considered as "young" populations.

Table 1 summarizes the 52 sources that are selected in the manner described above. In order to show the distribution of the sample sources in the Galaxy, in figure 1 we show maser positions in the CO l-v diagram obtained by Dame et al.(2001). As can be seen in figure 1, the sources are mostly located in the northern part of the Galactic plane. This is because the observing arrays (VERA, VLBA and EVN) are all located in the northern hemisphere. However, except for the concentration to the northern hemisphere, the sources are scattered well from the Galaxy center to the region beyond the anti-center, up to $l \sim 240^\circ$. To fill up the gap in the southern hemisphere, astrometry of maser sources with LBA (Australian VLBI array) and forthcoming SKA (Square Kilometer Array) will be effective, and this will be one of the most important future tasks in this kind of study.

As we will see in later sections, the whole set of 52 sources may include "outliers," which have large deviations from expected motions. Such a source could introduce systematic error into our results, and thus its effect should be investigated carefully. To do this, in later section (section 5), we will present results of various sample sets, in which some sources in list 1 are discarded depending on its degree of deviations. The source elimination will be made based on source's contribution to the likelihood, $P_i(\mathbf{O}_i|\mathbf{M})$ (see equation [3]): we create a new set of sample with $N-1$ sources by removing the source with smallest $P_i(\mathbf{O}_i|\mathbf{M})$ in the N-source sample. In this way, we will try various sets of samples with source numbers ranging from 52 to 44 (for details see section 5). In table 1 we mark the sources with their ranks in the likelihood.

3. Galaxy model

In order to derive fundamental Galaxy parameters, we use a simple Galaxy model in which motions of sources are basically in circular rotation with small systematic/random motions. As is widely used, the Local Standard of Rest (LSR) is set to be in circular rotation around the Galaxy center, which is described with two Galactic constants R_0 and Θ_0. Obviously R_0 is the distance between the Galaxy center and the LSR, and Θ_0 is the Galactic rotation velocity at the LSR. The ratio of Θ_0 to R_0 gives the Galactic angular velocity at the LSR Ω_0 (=Θ_0/R_0). In the following analyses, we use a set of R_0 and Ω_0, rather than a set of R_0 and Θ_0, as the Galactic constants to be solved because it is known that R_0 and Θ_0 are tightly correlated (e.g., Reid et al.2009b; McMillan and Binney 2010).

Regarding the Galactic rotation curve, we adopt two different rotation curves, a power law model and 2nd-order polynomial model. In the power law model (which is mainly studied here), the Galactic rotation velocity at any radius R is assumed to obey the following rotation low,

$$\Theta(R) = \Theta_0 \left(\frac{R}{R_0} \right)^{\alpha}. \quad (1)$$

Here α is the rotation curve index, and this parameter is to be solved in the following analysis to determine the shape of the rotation curve. Obviously, a flat rotation curve with $\Theta(R) = \Theta_0$ corresponds to $\alpha = 0$. Note that R is the radius in the cylindrical coordinate system defined with (R, β, Z), with its origin located at the Galaxy center (the notations here follow those in Reid et al. 2009b). On the other hand, in order to assess the effect of rotation curve models on Galactic parameter determinations, we also use the polynomial model described as,

$$\Theta(R) = \Theta_0 + a_0(R - R_0) + b_0(R - R_0)^2. \quad (2)$$

Here $a_0 = d\Theta/dR$ and $b_0 = (d^2\Theta/dR^2)/2$, respectively, and

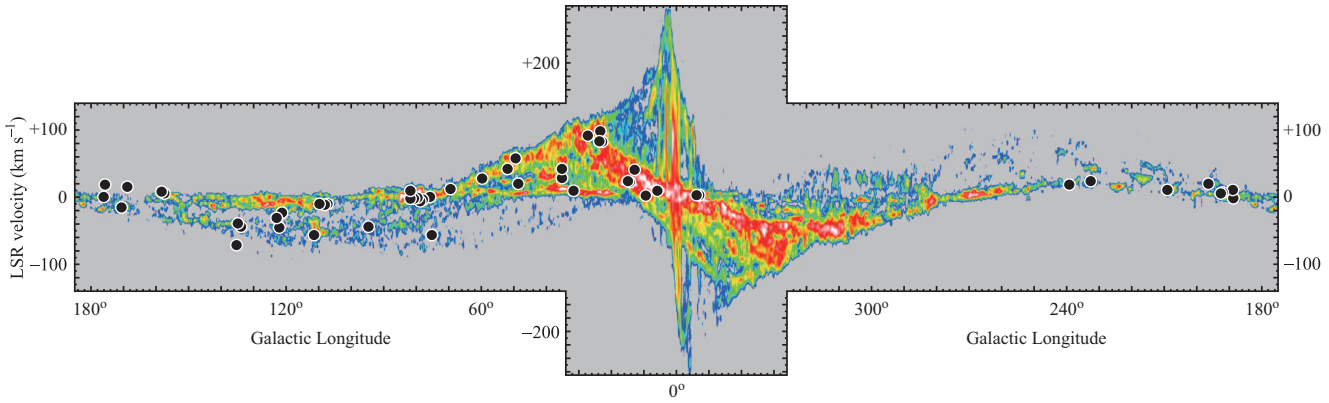

Fig. 1. Location of 52 maser sources for which accurate astrometric data are available (table 1), superposed on the longitude-velocity diagram of CO (Dame et al. 2001).

both coefficients are defined at $R = R_0$. This rotation curve contains two parameters while the power law model has only one. Thus, the polynomial rotation curve has a potential to give a better fit to the data, and we can test if inclusion of an additional parameter would alter the results based on the power law model.

We also include possible systematic motions of star-forming regions as model parameters to be solved, since Reid et al.(2009b) reported that high mass star-forming regions would lag behind Galactic rotation by ~ 15 km s^{-1}. In the present paper, this effect is re-considered in the same manner as Reid et al.(2009b) by including mean systematic motions of star-forming regions ($U_{\rm src}$, $V_{\rm src}$, $W_{\rm src}$). Note that the directions of $U_{\rm src}$, $V_{\rm src}$, $W_{\rm src}$ are defined at each source position, with $U_{\rm src}$ toward the Galaxy center, $V_{\rm src}$ toward the direction of Galactic rotation, and $W_{\rm src}$ toward the north Galactic pole, respectively.

In addition to the above parameters that describe the motions of maser sources in the Galaxy, we add one additional parameter to be solved for in our analysis: the V component of the Solar motion with respect to the LSR ($V_\odot$). As is widely known, the Sun is not at rest in the LSR frame but has its own peculiar motion with respect to the LSR. Based on the HIPPARCOS observations of local stellar motions and distances, Dehnen and Binney (1998) obtained the Solar motion with respect to the LSR as, ($U_\odot$, $V_\odot$, $W_\odot$) = (10.00±0.36, 5.25±0.62, 7.17±0.38) km s^{-1}, reducing the V component of the Solar motion by ~ 10 km s^{-1} from the classical value of $V_\odot$=15.4 km s^{-1} (Kerr & Lynden-Bell 1986). However, recent reanalyses of the data reported that the V component of the Solar motion by Dehnen & Binney (1998) was an underestimate and that an upward modification of $V_\odot$ is required by ~ 7 km s^{-1} (Schönrich et al. 2010), yielding $V_\odot \sim 12$ km s^{-1}. Interestingly, this upward modification reduces the rotation velocity lag of the star-forming regions (McMillan & Binney 2010). Therefore, the lag parameter $V_{\rm src}$ and $V_\odot$ are correlated to each other to some extent, and we include $V_\odot$ as possible parameter (fixed or solved depending on models considered) to see how our results are affected. Note that the other two components of the Solar motion ($U_\odot$, $W_\odot$) are assumed to be well-determined, since previous studies were consistent between each other (e.g., Kerr & Lynden-Bell 1986; Dehnen & Binney 1998; Aumer & Binney 2009; Schönrich et al. 2010). Throughout the present paper, we simply take $U_{\rm sun}$ and $W_{\rm sun}$ of Dehnen & Binney (1998). Table 2 summarizes the parameters to be solved for in the present analyses.

4. Analysis

To obtain the best estimates of the Galactic parameters described above, we utilize a Markov chain Monte Carlo (MCMC) method with the Metropolis algorithm. To do this, first we define the likelihood function as

$$L(\mathbf{M}) = \prod_i P_i(\mathbf{O}_i|\mathbf{M}). \quad (3)$$

Here $P_i(\mathbf{O}_i|\mathbf{M})$ is the conditional probability of finding observables $\mathbf{O}_i$ given a set of model parameters $\mathbf{M}$. $\mathbf{O}_i$ represents the observables for the i-th source, a detailed description of which is provided later. The model $\mathbf{M}$ represent the model parameters described in the previous section: for the power law rotation curve,

$$\mathbf{M} = (R_0, \Omega_0, \alpha, U_{\rm src}, V_{\rm src}({\rm or}\, V_\odot), W_{\rm src}), \quad (4)$$

or for the polynomial rotation curve case,

$$\mathbf{M} = (R_0, \Omega_0, a_0, b_0, U_{\rm src}, V_{\rm src}({\rm or}\, V_\odot), W_{\rm src}). \quad (5)$$

Note that as we will see later there is a strong correlation between $V_{\rm src}$ and $V_\odot$, and thus these two parameters are not solved for at the same time, but one of them are fixed while the other is being solved for.

In a practical MCMC method, we calculate the likelihood $L(\mathbf{M})$ based on the equation (3) for a current set of model parameters $\mathbf{M}$. Then, the next set of $\mathbf{M}'$ is calculated by adding a small random fluctuations to the previous $\mathbf{M}$, and the likelihood $L'(\mathbf{M}')$ is calculated. If $L'(\mathbf{M}') \geq L(\mathbf{M})$, the next parameter $\mathbf{M}'$ is accepted. If not, we draw a random variable u, which has a uniform probability between 0 and 1, and we accept the next parameter $\mathbf{M}'$ in case of $L'(\mathbf{M}')/L(\mathbf{M}) > u$. In other case (i.e., $L'(\mathbf{M}')/L(\mathbf{M}) \leq u$), the next parameter set is rejected and the parameter set remains at the previous one

Table 2. Summary of the Galactic parameters used in the present paper.

parameter	notes
R_0	the distance from the Sun to the Galaxy center
Ω_0	Angular rotation velocity at the LSR ($\Omega_0 = \Theta_0/R_0$)
α	rotation curve index defined as $\Theta(R) = \Theta_0(R/R_0)^\alpha$
a_0, b_0	rotation curve coefficients defined as $\Theta(R) = \Theta_0 + a_0(R-R_0) + b_0(R-R_0)^2$
$U_{\rm src}$	mean peculiar motion of SFRs toward the Galaxy Center
$V_{\rm src}$	mean peculiar motion of SFRs toward the direction of Galactic rotation
$W_{\rm src}$	mean peculiar motion of SFRs toward the north Galactic pole
$V_\odot$	V component of the Solar motion (toward the Galactic rotation)

$\mathbf{M}$. Above procedures are iterated for a large number of trials (typically for $\sim 10^5$). The best estimates of $\mathbf{M}$ and their error bars are obtained by taking means and standard deviations of the samples of $\mathbf{M}$ in the MCMC trials, after removing early trials in the initial "burn-in" phase, which is set to be the first 10% of the trials. Note that these procedures correspond to a MCMC method with a uniform *a priori* probability distribution of model parameters, namely $P(\mathbf{M}) = const.$ The reason for adopting a constant prior probability is that in the present paper we want to constrain Galactic parameters based only on VLBI astrometry data of star-forming regions rather than partially relying on other results in previous studies. However, since the parameters $\mathbf{M}$ are well constrained to relatively narrow ranges in the final results of MCMC (see next section) the choice of a different *a priori* probability (such as uniform probability in the logarithm) would not alter the main results presented here.

For the observables, $\mathbf{O}_i$ (which is for the i-th source) is given as

$$\mathbf{O_i} = (V_{\rm LSR}, \mu_l, \mu_b)_i. \quad (6)$$

Here $V_{\rm LSR}$ is the radial velocity with respect to the LSR (based on the conventional Solar motion), μ_l and μ_b are the two components of proper motions along the Galactic coordinate l and b. We adopted these quantities as observables because they are commonly used, but here we note that they are not in the exactly same frame: while $V_{\rm LSR}$ is measured in the conventional LSR frame, μ_l and μ_b are observed in the heliocentric frame. When MCMC analyses are done in later section, of course μ_l, μ_b and $V_{\rm LSR}$ are converted to the appropriate LSR frame by using the adopted Solar motion. We also note that VLBI astrometry provides the full 6-dimensional coordinates in the phase space, but here the source coordinates l and b are not considered as "observables".

In order to calculate the conditional probability $P_i(\mathbf{O}_i|\mathbf{M})$ in equation (3), here we simply adopt Gaussian for the probability distribution of finding an observable given the model $\mathbf{M}$ and the source parallax π_i, namely,

$$P(x_i|\mathbf{M},\pi_i) = \frac{1}{\sqrt{2\pi\sigma^2}} \exp\left(\frac{-(x_{\rm obs}-x_{\rm model})^2}{2\sigma^2}\right), \quad (7)$$

where $x_{\rm obs}$ is the observable (corresponding to $V_{\rm LSR}$, μ_l, and μ_b of the i-th source). The model value $x_{\rm model} = x_{\rm model}(\mathbf{M},\pi_i)$ is calculated based on the Galactic model $\mathbf{M}$ as well as the observed source parallax π_i. The conditional probablity $P_i(\mathbf{O}_i|\mathbf{M})$ in equation (3) can be obtained by multiplying the Gaussian distribution in equation (7) for the three parameters ($V_{\rm LSR}$, μ_l, and μ_b) and also by integrating over the possible parallax range of π. The integration over the possible range of π is done by adopting Gaussian distribution of π with a standard deviation given by the observational uncertainty listed in table 1. Then, the likelihood in equation (3) is evaluated by multiplying the conditional probability $P_i(\mathbf{O}_i|\mathbf{M})$ for all the sources in the sample.

The standard deviation σ in equation (7) is determined by considering both the errors in the observations and the uncertainties in model estimates. In addition to the observational errors listed in table 1, we include the effect of source random motion, which is assumed to be isotropic with a 1-dimensional velocity dispersion of σ_v. This velocity dispersion accounts for the turbulent motion in the molecular clouds and also systematic difference of maser source motions from proto-stars, and throughout the paper we set $\sigma_v = 7$ km s^{-1} unless otherwise noted. As for radial velocities, observational error of the LSR velocity $\sigma_{\rm LSR,obs}$ and the source velocity dispersion σ_v is summed in quadrature to calculate σ in equation (7) as $\sigma^2_{\rm LSR} = \sigma^2_{\rm LSR,obs} + \sigma^2_v$. For proper motions, again we add the observational error $\sigma_{\rm obs}$ and the random motions in quadrature to obtain $\sigma_{\mu\, l,b} = \sqrt{\sigma^2_{{\rm obs}\, l,b} + (\sigma_v/D)^2}$.

5. Results

In order to obtain the best estimates of the Galactic parameters, we conducted several MCMC analyses for different sample data sets as well as different set of model parameters. First in section 5.1, we present the results with different samples (while fixing model parameters), and then in section 5.2 we treat cases with different model parameters.

5.1. Results with varying number of sample sources

Table 3 summarizes the MCMC results for different samples, with the source number varying from 52 to 44. Here in table 3, the model parameters are Galactic constants R_0 and Ω_0, the power-law index of the rotation curve, α, the mean SFRs motions (with respect to the Galactic rotation) $U_{\rm src}$, $V_{\rm src}$ and $W_{\rm src}$. Note that the Solar motion $V_\odot$ is fixed to 5.25 km $^{-1}$, adopting the results by Dehnen & Binney (1998). The effect of varying $V_\odot$ and the rotation curve shape will be examined later. Error bars in table 3 show statistical error (1-σ) obtained with the MCMC analyses. In table 4, we also show the correlation coefficients between Galactic parameters for the sample of 49 sources as an example (result 4 in table 3). As seen in table 4,

Table 3. MCMC results of the Galactic parameters for various sample sets

result ID	# of source	R_0 (kpc)	Ω_0 (km/s/kpc)	α	$U_{\rm src}$ (km s^{-1})	$V_{\rm src}$ (km s^{-1})	$W_{\rm src}$ (km s^{-1})	$V_\odot$ (km s^{-1})	χ^2/d.o.f.
1	52	8.27±0.42	29.98±0.64	+0.05±0.02	1.1±1.3	−14.8±1.2	−0.6±1.0	5.25*	494/150
2	51	8.20±0.41	29.89±0.66	+0.05±0.02	0.8±1.4	−14.6±1.2	−1.9±1.0	5.25*	410/147
3	50	8.40±0.42	30.37±0.76	+0.04±0.02	0.4±1.4	−14.3±1.2	−2.0±1.1	5.25*	388/144
4	49	7.84±0.40	30.61±0.75	+0.00±0.02	0.6±1.4	−13.1±1.2	−1.9±1.0	5.25*	353/141
5	48	7.90±0.40	30.33±0.71	+0.00±0.02	1.4±1.4	−13.6±1.2	−1.8±1.1	5.25*	333/138
6	47	7.91±0.38	30.73±0.76	+0.00±0.02	1.4±1.4	−13.6±1.3	−1.5±1.1	5.25*	327/135
7	46	7.94±0.42	30.59±0.76	+0.01±0.02	1.2±1.4	−13.2±1.3	−1.3±1.1	5.25*	312/132
8	45	7.93±0.42	30.70±0.77	+0.02±0.02	0.8±1.5	−12.7±1.3	−1.0±1.1	5.25*	303/129
9	44	8.04±0.42	30.71±0.76	+0.02±0.02	0.8±1.5	−12.5±1.3	−0.8±1.1	5.25*	288/126

* : fixed parameter

For result 1, all 52 sources are used. For other samples, following sources are removed one-by-one from result 2 to 9: IRAS 20126+4104, G48.61+0.02, G9.62+0.20, T-Tau/Sb, AFGL 2591, NGC 7538, IRAS 06061+2151, and AFGL 2789. Error bars show statistical uncertainties obtained with the MCMC analyses.

Table 4. Correlation coefficients between Galactic parameters for result 4 (49 sources)

	R_0	Ω_0	$U_{\rm src}$	$V_{\rm src}$	$W_{\rm src}$	α
R_0	1.000	−0.164	0.096	−0.397	0.065	0.494
Ω_0		1.000	−0.576	−0.052	−0.006	−0.048
$U_{\rm src}$			1.000	0.027	0.023	0.002
$V_{\rm src}$				1.000	−0.031	−0.148
$W_{\rm src}$					1.000	0.022
α						1.000

Table 5. MCMC results of the Galactic parameters for different model parameters

result ID	# of source	R_0 (kpc)	Ω_0 (km/s/kpc)	α or (a_0, b_0)[c]	$U_{\rm src}$ (km s^{-1})	$V_{\rm src}$ (km s^{-1})	$W_{\rm src}$ (km s^{-1})	$V_\odot$ (km s^{-1})	χ^2/d.o.f.
10	52	8.27±0.42	29.98±0.64	+0.05±0.02	1.1±1.3	−14.8±1.2	−0.6±1.0	5.25*	494/150
11	52	8.25±0.40	29.15±0.63	+0.05±0.02	1.1±1.4	−8.1±1.2	−0.5±1.0	12.0*	497/150
12	52	8.25±0.40	28.10±0.66	+0.05±0.02	1.3±1.4	0.0*	−0.5±1.0	19.9±1.2	499/150
13	49	7.84±0.40	30.61±0.75	+0.00±0.02	0.6±1.4	−13.1±1.2	−1.9±1.0	5.25*	353/141
14	49	7.82±0.41	29.60±0.74	+0.00±0.02	0.8±1.4	−6.3±1.2	−1.9±1.1	12.0*	353/141
15	49	7.77±0.38	28.89±0.71	+0.00±0.02	0.7±1.4	0.0*	−1.9±1.1	18.2±1.2	357/141
16	46	7.94±0.42	30.59±0.76	+0.01±0.02	1.2±1.4	−13.2±1.3	−1.3±1.1	5.25*	312/132
17	46	7.93±0.40	29.74±0.74	+0.01±0.02	1.3±1.4	−6.5±1.3	−1.3±1.1	12.0*	314/132
18	46	7.90±0.38	28.86±0.76	+0.01±0.02	1.3±1.4	0.0*	−1.3±1.1	18.3±1.2	315/132
19	49[a]	7.68±0.28	30.61±0.53	−0.00±0.02	0.5±1.0	−12.8±0.9	−1.8±0.8	5.25*	603/141
20	49[b]	7.97±0.51	30.50±0.97	+0.01±0.03	1.0±2.0	−13.3±1.7	−1.9±1.5	5.25*	192/141
21	49	7.72±0.41	30.58±0.71	−0.1±0.7 0.1±0.2	0.6±1.4	−13.2±1.3	−1.9±1.0	5.25*	361/140
22	49	7.70±0.40	29.71±0.71	−0.1±0.7 0.1±0.2	0.7±1.4	−6.5±1.3	−1.9±1.1	12.0*	367/140
23	49	7.70±0.40	28.91±0.71	−0.1±0.7 0.1±0.2	0.6±1.4	0.0*	−1.9±1.1	18.3±1.3	364/140

* : fixed parameter
a : with $\sigma_v = 5$ km s^{-1} instead of 7 km s^{-1}.
b : with $\sigma_v = 10$ km s^{-1} instead of 7 km s^{-1}.
c : through models 10 to 20, α (non-dimensional RC index), and for models 21–23, upper raw corresponds to $a_0 = d\Theta/dR$ (km/s/kpc), and lower raw corresponds to $b_0 = (d^2\Theta/dR^2)/2$ (km/s/kpc^2), respectively (values defined at $R = R_0$)

some correlation coefficients exceed 0.2, indicating relatively large correlation between parameters. Part of such correlation can be seen, for instance, in figures 2a, 2c and 2f, where cases with higher R_0 for results 1–3 provide higher α and lower $V_{\rm src}$, but note that the results presented here are determined including the effect of such correlation. Of course, the strongest correlation exists between $V_\odot$ and $V_{\rm src}$ (which is not shown in table 4), which prevents us from determining these two parameters at the same time.

As is described in section 2, the full source list consists of 52 sources for which results of precise astrometry are available. However, in the sample sources, there likely exist "outliers," which have large deviations from the model-predicted radial velocity and/or proper motions. To investigate the effect of such outliers, we ran MCMC analyses for several sets of sample sources by eliminating possible outliers one-by-one. The elimination was done based on the conditional probability $P_i(\mathbf{O}_i|\mathbf{M})$: a new sample of $N-1$ sources was created by eliminating the source with the smallest value of $P_i(\mathbf{O}_i|\mathbf{M})$ in the MCMC results for the N-source sample. In table 3 (and 5) we also provide χ^2 and degrees of freedom (d.o.f.) for each model (rather than the likelihood), because they are fairly useful to see the effect of outliers.

As we will see later in this section (e.g, table 5), the parameters related to the Galactic rotation velocity such as Ω_0, $V_{\rm src}$ and $V_\odot$ are tightly correlated with each other, and thus will be treated in further detail in next subsection (by solving for $V_{\rm src}$ or $V_\odot$). Other parameters such as R_0, α, $U_{\rm src}$, and $W_{\rm src}$ are independent of the choice of model parameters, and thus the results listed in table 3 give strong constraints on these parameters. In figures 2, we show resultant model parameters with the number of sample sources $N_{\rm src}$ varying from 52 to 44: R_0, Ω_0, α, $U_{\rm src}$, $V_{\rm src}$, $W_{\rm src}$, and χ^2 versus the number of the sources $N_{\rm src}$. For reference, the sources with small conditional probability are also labeled in table 1. The effects of "outliers" can been seen in figures 2. For instance, in figure 2d the value χ^2 rapidly increases beyond 50, and χ^2 of the full sample (52 objects) is nearly 500 while it is around 350 for 49 objects (see also results 1 and 4 in table 3). Therefore, it is likely that at least these three sources (IRAS 20126+4104, G48.61+0.02, G9.62+0.20) are indeed outliers, and these three sources may be better to be excluded from the sample to obtain the best estimates of the Galactic parameters. In fact, previous studies reported large peculiar motions for these sources: G48.61+0.02 was found to be associated with supernova W51C (Nagayama et al. 2011), and thus the peculiar motion is likely to be originated from a supernova explosion. Sanna et al.(2009) suggested that large deviation (~ 40 km s^{-1}) of G9.62+0.02 from the Galactic rotation may be due to the bar potential in the inner Galaxy. The cause of relatively large non-circular motion of IRAS 20126+4104 is unknown, but Moscadelli et al.(2011) already pointed out an existence of that at $\sim$20 km s^{-1} level when a standard rotation curve is considered.

Due to the effect of these outliers, the best-estimate values of some parameters such as R_0, α, etc. indeed vary with decreasing $N_{\rm src}$ from 52 to 49 (as in figures 2). On the other hand, reducing $N_{\rm src}$ further (below 48) do not alter the best-estimates of those parameters as much. Therefore, one can expect that the sample with $\sim$48 sources do not contain "outliers."

Although at least the top-three sources in terms of low conditional probability are highly likely to be outliers, here we do not simply eliminate these outliers from our samples, but we take a rather conservative approach by taking both samples with/without outliers into account and consider the effects of outliers as possible systematic error in our analyses. For instance, in figure 2a, the Galaxy center distance R_0 is determined with an statistical uncertainty $\sigma_{\rm stat}$ of 0.4 kpc (e.g., for $N_{\rm src} \sim 48$). On the other hand, the best estimated of R_0 for $N_{\rm src} = 50$ and 52 differs from that for $N_{\rm src} = 48$ slightly beyond the statistical error bar. This clearly demonstrates the systematic effect of outliers, and we regard this scatter as the systematic error in our estimates of the Galactic parameters. In practice, we obtain the best estimate of the parameters by taking the mean of the results with the sample source number varying from 44 to 52, and also calculate its standard deviation as the systematic error $\sigma_{\rm sys}$. Then we evaluate the final uncertainty by summing up in quadrature both typical statistical error (taken as the mean of statistical error bars for $N_{\rm src}$ ranging from 44 to 52) and systematic error $\sigma_{\rm sys}$. Note that here the selection of the smallest number of the sample sources to be used is rather arbitrary, but in the present analyses we adopt 44 for the minimum number of the sources. In fact lowering the number of the sample further would not alter the resultant parameters drastically, but the uncertainty would be slightly increasing due to statistical effect.

The best estimates of Galactic parameters obtained in that way are also plotted in each panel of figures 2 by dotted lines showing the possible range. For the best estimate of R_0, we obtained

$$R_0 = 8.05 \pm 0.45 \ {\rm kpc}. \tag{8}$$

This is 5%-level determination of the most fundamental Galactic constant R_0. As we will see in discussion later, this is consistent with other recent studies of R_0 such as using motions of stars around the Galaxy center or variable stars, but we note that our result is independent of others and provides another constraint on the distance to the Galaxy center.

The rotation curve index α is also tightly constrained to be

$$\alpha = 0.022 \pm 0.029. \tag{9}$$

The index is 0 within the error bar, confirming that the rotation curve of the Galaxy is basically flat in the regions where our samples are distributed (Galacto-centric radius of 4 to 13 kpc). The use of the full sample gives a marginally positive value of α of 0.05, but we note that $\alpha = 0.05$ results in a rise of rotation velocity only by $\pm$3 % between Galacto-centric radius between 5 and 15 kpc. Hence, even in the maximum case of α, Galactic rotation curve flatness is $\pm$3% level in those regions.

The U and W components of the source non-circular motions are also well constrained here, and we obtained

$$U_{\rm src} = 0.95 \pm 1.46 \ {\rm km\,s^{-1}}, \tag{10}$$

$$W_{\rm src} = -1.41 \pm 1.19 \ {\rm km\,s^{-1}}. \tag{11}$$

The mean inward motion $U_{\rm src}$ is obtained to be 0 within the error bar. Also, the mean perpendicular motion $W_{\rm src}$ is found to be practically 0 within the error bars, being independent of the models. This is rather natural when one considers the symmetry of Galactic disk along the Galactic latitude.

These parameters do not depend on the various models considered in the next section, and we take them as our final results for these parameters. Regarding other parameters, from figures 2 we also obtained $\Omega_0 = 30.43 \pm 0.80$ km s^{-1} kpc^{-1}, $V_{\rm src} = -13.60 \pm 1.49$ km s^{-1}, but as will be seen in the next subsection, we have to consider other systematic effects to obtain the final results.

5.2. Results with changing model parameters

In this subsection we present the MCMC results of the Galactic parameters by choosing different model parameter sets and also different rotation curves. Table 5 summarizes the results, again presenting results of the best estimates of the parameters, as those in table 3. In table 5 results 10–12 are a family of the best estimates for the full sample of 52 sources, with different treatment of $V_{\rm src}$ and $V_\odot$: in result 10 we adopt $V_\odot$=5.25 km $^{-1}$ (Dehnen & Binney 1998, note that result 10 is identical to result 1 in table 3), while in result 11 $V_\odot$=12.0 km $^{-1}$ (Schönrich et al. 2010) is adopted. In both results 10 and 11, $V_{\rm src}$ is considered as a parameter to be solved for. As seen in results 10 and 11, the SFRs lag velocities (negative $V_{\rm src}$) differ by nearly the same amount with the change in adopted $V_\odot$, indicating strong correlation between $V_{\rm src}$ and $V_\odot$. On the other hand, in result 12, instead we fixed $V_{\rm src}$=0 km s^{-1} (no SFRs lag) and solved for the Solar motion $V_\odot$. In other words, in result 12, the apparent slow rotation of SFRs is totally attributed to the Solar peculiar motion. Results 13–15, and 16–18 are other families of the results similar to results 10–12, but for different numbers of the sample sources: results 13–15 are for the sample of 49 sources, and results 16–18 are for the sample of 46 sources (note that results 4 and 13, and results 7 and 16 are identical to each other, respectively). The elimination of sources from the full sample is conducted based on the conditional probability $P_i(\mathbf{O}_i|\mathbf{M})$, as is already described in 5.1. These results with different number of sources are again presented to evaluate the effect of samples with/without outliers.

Results 19 and 20 are to investigate the dependence of the results on the adopted value of 1-dimensional velocity dispersion of SFRs (σ_v): throughout the paper, σ_v=7 km s^{-1} is adopted, but only for results 19 and 20, this is altered to 5 or 10 km s^{-1}, respectively ($V_\odot$=5.25 km s^{-1} is adopted for both results 19 and 20). Results 19 and 20 should be compared with results 13, because they are based on the same sample and parameters with only difference in σ_v. As can be seen in table 5, the results 19, 20 and 13 are fairly consistent with each other. The only difference is the size of statistical error bars and the value of χ^2, as is expected in case of using different σ_v : result 19 gives χ^2 of 603 against d.o.f. of 141, and result 20 gives χ^2 of 192. They are to be compared with result 13 provides χ^2 of 353. In terms of reduced χ^2 ($=\chi^2/{\rm d.o.f}$), σ_v of 10 km s^{-1} seems too large, and our choice of $\sigma_v = 7$ km s^{-1} seems more reasonable. The reduced χ^2 may indicate that $\sigma_v = 5$ km s^{-1} is reasonbale, but here we conservatively adopt $\sigma_v = 7$ km s^{-1} because the use of too small σ_v could lead to underestimation of statistical error. Note that the adopted value of $\sigma_v = 7$ km s^{-1} is similar to those in the previous studies: for instance, Reid et al.(2009b) used 7 km s^{-1} for σ_v, and McMillan & Binney (2010) solved σ_v by setting it as a parameter to be estimated, and obtained σ_v from 7 to 10 km s^{-1} depending on their models.

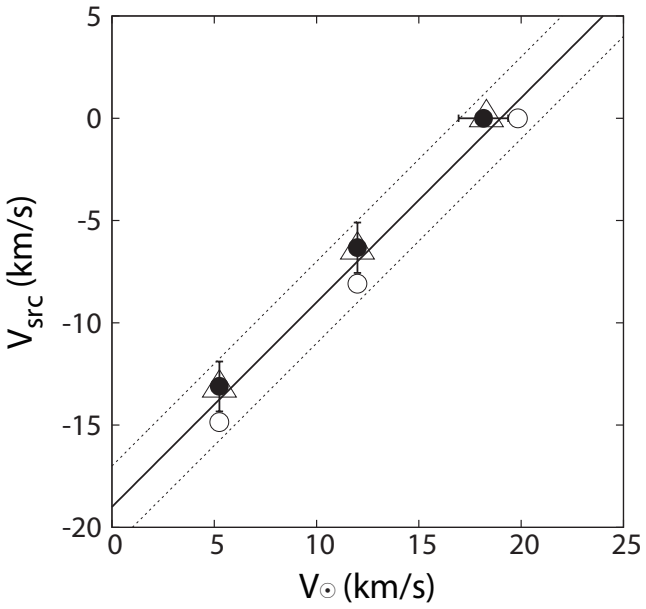

Fig. 3. Correlation between $V_\odot$ and $V_{\rm src}$. Open circles are those for results 10–12 in table 5, filled circles with error bars for results 13–15, and open triangles for results 16–18, respectively. Thin line corresponds to the best fit relation of $V_{\rm src} = V_\odot - 19(\pm 2)$ km s^{-1}, with dotted lines showing the error bar range.

The last three results (21–23) in table 5 are those for using different rotation curve models. Reid et al.(2009b) and McMillan & Binney (2010) suggested that the Galactic parameters also depend on choice of rotation curve shape. In most cases in table 3 and 5 we used a power-law rotation curve. In order to see how results would be altered with a different rotation curve, we adopt the 2nd-order-polynomial rotation curve in equation (2) for results 21-23. This rotation curve has two parameters, while a power-law rotation curve has only one parameter. However, as can be seen in table 5, the use of a different rotation curve does not change our results drastically. This may indicate that the shape rotation curve determined with the current sample is basically well-represented by a simple function such as the one-parameter power-low model.

From table 5, one can see that the parameters R_0, α, $U_{\rm src}$ and $W_{\rm src}$ are not strongly dependent on the choice of $V_\odot$ or $V_{\rm src}$. For instance, from results 11 to 20, R_0 ranges from 7.7 to 8.3 kpc, but basically this is the sample effect: in fact, the best estimate of R_0 remains unchanged within a family of results based on the same sample (such as results 10–12, 13–15 etc.). The variation of R_0 for results 10–23 thus originates from the difference in the number of sources (and hence inclusion/exclusion of outliers). The best estimate of R_0 obtained in 5.1, which is R_0=8.05$\pm$0.45 kpc including systematic error, fully covers the range of R_0 in table 5. Therefore, as we described in the previous subsection, we can consider the value of R_0 obtained in the previous subsection as the final value for the current study. In addition to R_0, the same applies to α, $U_{\rm src}$ and $W_{\rm src}$, and the best estimates obtained in section 5.1 cover the full ranges of these parameters in table 5.

On the other hand, in table 5, there are strong correlations between the Solar peculiar motion $V_\odot$, the mean source mo-

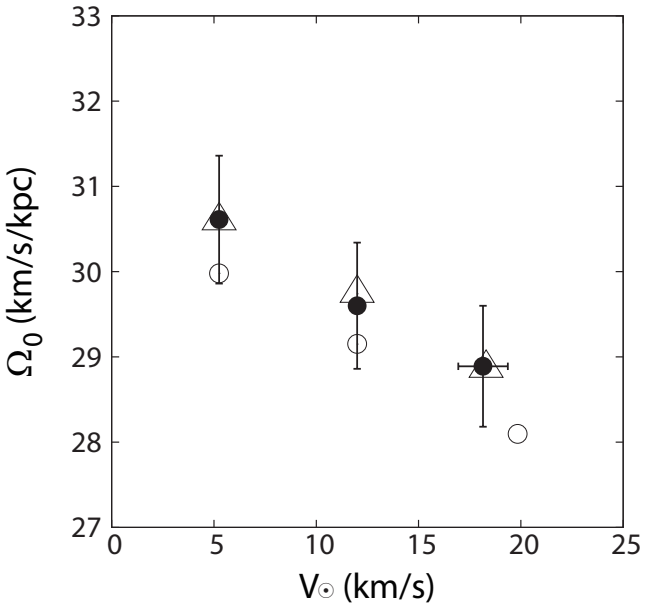

Fig. 4. Correlation between $V_\odot$ and Ω_0. Open circles are those for results 10–12 in table 5, filled circles with error bars for results 13–15, and open triangles for results 16–18, respectively.

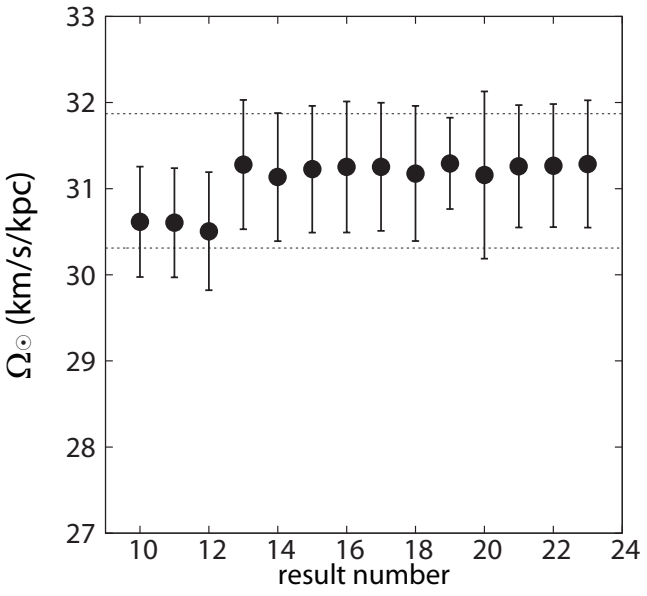

Fig. 5. Angular rotation velocity of the Sun, $\Omega_\odot$, obtained for results 10–23 in table 5 (filled circles with error bars). Horizontal axis is the result ID, running from 10 to 23. Dotted lines show the possible range of $\Omega_\odot$ for our best estimate, $\Omega_\odot = 31.09 \pm 0.78$ km s^{-1} kpc^{-1}.

tion in the rotational direction $V_{\rm src}$, and the angular velocity of the LSR Ω_0. One can see this correlation by comparing the results for the same sample but with different $V_\odot$ or $V_{\rm src}$ (e.g., results 10–12). To clearly show this situation, in figure 3 we show the relation between $V_\odot$ and $V_{\rm src}$ for the results in table 5. The open circles in figure 3 are for results 10–12, filled circles (with error bars) for results 13–15, and open triangles for results 16–18, respectively. As seen in figure 3, the relation between $V_\odot$ and $V_{\rm src}$ can be approximated by a linear function, with $V_{\rm src} = V_\odot - 19$ km s^{-1} (thin line in figure 3). When one compares χ^2 values with the three results based on the same sample (e.g., models 10–12, 13–15, ...), there is little difference in χ^2, indicating that our results do not show any preference for a particular choice of $V_{\rm src}$ and $V_\odot$. Therefore, at this stage, the only thing we can constrain is that these two quantities must satisfy the following relation

$$V_{\rm src} = V_\odot - 19\,(\pm 2)\ {\rm km\ s^{-1}} \qquad (12)$$

The allowed region of ($V_\odot$, $V_{\rm src}$) with the above error bar (± 2 km s^{-1}) is also shown in figure 3 with dotted lines. If $V_\odot = 5.25$ km s^{-1} is adopted to this relation, the star-forming regions lag behind the Galactic rotation by ~ 14 km s^{-1}, confirming the earlier suggestion by Reid et al.(2009b). On the other hand, an upward modification of $V_\odot$ by Schönrich et al. (2010) with $V_\odot = 12.0$ km s^{-1} reduces the lag down to ~ 7 km s^{-1} level. Only $V_\odot$ of ~ 20 km s^{-1} can lead to no lag case, but this solar motion is larger than the classical IAU value of the Solar motion, with $|V| = 20$ km s^{-1} toward (18^h, 30°) in B1900 (e.g., Kerr & Lynden-Bell 1986), corresponding to $V_\odot = 15$ km s^{-1}. Hence, this should be taken to be an extreme case, and probably reality would lie among these cases (e.g., up-ward modified $V_\odot$ with some rotation lag). The tight correlation between $V_\odot$ and $V_{\rm src}$ can be simply attributed to the fact that the observed sources motions are relative to that of the Solar system and hence the effect of the Solar motion and lag of star-forming regions are still degenerated.

Table 6. Additional Galactic parameters

model ID	$V_\odot$ km s^{-1}	$V_\odot - V_{\rm src}$ km s^{-1}	$\Omega_\odot$ km s^{-1} kpc^{-1}	Θ_0 km s^{-1}
10	5.25	20.1±1.2	30.61±0.64	247.9±13.7
11	12.0	20.1±1.2	30.60±0.63	240.5±12.8
12	*	19.9±1.2	30.50±0.69	231.8±12.5
13	5.25	18.4±1.2	31.28±0.75	240.0±13.6
14	12.0	18.3±1.2	31.13±0.74	231.5±13.4
15	*	18.2±1.2	31.23±0.74	224.5±12.3
16	5.25	18.5±1.3	31.25±0.76	242.9±14.2
17	12.0	18.5±1.3	31.25±0.74	235.8±13.3
18	*	18.3±1.2	31.18±0.78	228.0±12.5
19	5.25	18.0±0.9	31.29±0.53	235.1± 9.5
20	5.25	18.5±1.7	31.16±0.97	243.1±17.4
21	5.25	18.5±1.3	31.26±0.71	236.1±13.7
22	12.0	18.5±1.3	31.27±0.71	228.8±13.1
23	*	18.3±1.3	31.29±0.74	222.6±12.8

* denotes that $V_\odot$ is solved for by setting $V_{\rm src} = 0$ km s^{-1}. The resultant $V_\odot$ is identical to the value in the right column of $V_\odot - V_{\rm src}$. Θ_0 is calculated using the relevant values of R_0 and Ω_0 in table 5.

The correlation between $V_{\rm src}$ and $V_\odot$ also affects the angular rotation velocity of the LSR Ω_0. For instance, Ω_0 simply decreases in results 10–12 as $V_\odot$ increases, and the same trends are found in results 13–15 and 16–18 in table 5. Figure 4 illustrates this correlation between $V_\odot$ and Ω_0, with the same symbols as in figure 3. Here again $V_\odot$ and Ω_0 show a linear

Table 7. Summary of Galactic parameters obtained in the present paper. Error bars indicated here include systematic errors.

R_0	8.05±0.45	kpc
$\Omega_\odot$	31.09±0.78	km s^{-1} kpc^{-1}
α	0.022±0.029	
$U_{\rm src}$	0.95±1.46	km s^{-1}
$V_{\rm src}$	$V_\odot - 19\ (\pm 2)$	km s^{-1}
$W_{\rm src}$	-1.41 ± 1.19	km s^{-1}

trend. Considering this situation, it is useful to introduce a following new Galactic parameter

$$\Omega_\odot \equiv \Omega_0 + \frac{V_\odot}{R_0}, \tag{13}$$

which is the angular velocity of the Sun. Table 6 summarizes the derived $\Omega_\odot$ and other parameters such as $V_\odot - V_{\rm src}$ and Θ_0, based on the results in table 5. Also, figure 5 shows $\Omega_\odot$ for results 10–23 in table 5. As seen in figure 5, the resultant $\Omega_\odot$ shows only weak dependence on the results (number of the source, choice of $V_\odot$ etc.), and thus is readily constrained well in the present study. As was done for R_0 determination in the previous subsection, from figure 5, $\Omega_\odot$ is determined as

$$\Omega_\odot = 31.09 \pm 0.78\,{\rm km\,s^{-1}\,kpc^{-1}}. \tag{14}$$

Here again the error bar includes systematics due to the effect of outliers. This is consistent with the direct measurement of Sgr A* motion along the Galactic plane carried out by Reid & Brunthaler (2004), who obtained $\mu_l = 6.379 \pm 0.024$ mas yr^{-1}, or the angular rotation velocity $\Omega_\odot$ of 30.24±0.11 km s^{-1} kpc^{-1}. Note that while $\Omega_\odot$ is well constrained, in table 6 Θ_0 still remains relatively uncertain. In fact, in table 6, the full possible range of Θ_0 is 223 – 248 km $^{-1}$. Hence the determination of precise $V_\odot$ and Θ_0 is still an important issue for future observations. In table 7, we summarize final values and relations for Galactic parameters in the present study. The error bars in table 7 include both statistical and systematic error, as already discussed in this section.

6. Galactic parameter comparisons

6.1. R_0

In the previous section, we have obtained the Galaxy center distance to be $R_0 = 8.05 \pm 0.45$ kpc, with the error bar including systematics due to possible "outliers". This result is fully consistent with recent studies of R_0. For instance, the review paper by Reid (1993) summarized the previous studies of R_0 and provided $R_0 = 8.0 \pm 0.5$ kpc. Observations of stellar orbits around Sgr A* also provided the distance to the Galaxy center as $R_0 = 8.4 \pm 0.4$ kpc (Ghez et al. 2008) and $R_0 = 8.33 \pm 0.35$ kpc (Gillessen et al. 2009). Earlier analysis of Galactic structure based on maser astrometry (Reid et al. 2009b) also reported $R_0 = 8.4 \pm 0.6$ kpc. Period-Luminosity relation for Mira also suggests $R_0 = 8.24 \pm 0.08|_{\rm stat} \pm 0.42|_{\rm sys}$ kpc (Matsunaga et al. 2009). All these studies are consistent within error bars and thus the result in the present paper confirms that R_0 is between 8 and 8.5 kpc.

6.2. $\Omega_\odot$ and Ω_0

The most direct determination of $\Omega_\odot$ is the apparent proper motion of Sgr A* along the Galactic plane: assuming that the Sgr A* is at rest at the center of the Galaxy, its proper motion directly reflects the sum of the Galactic rotation at the LSR and the Solar motion with respect to the LSR. As already mentioned in the previous section, our result of $\Omega_\odot = 31.09 \pm 0.78$ km s^{-1} kpc^{-1} is consistent with the Sgr A* motion obtained by Reid & Brunthaler (2004), which was $\Omega_\odot$ of 30.24±0.11 km s^{-1} kpc^{-1}. Note that our astrometry data does not include the proper motion of Sgr A* itself, and hence these two studies are totally independent. This consistency assures that the Sgr A* is indeed at rest at the Galaxy center, with an upper limit of its in-plane motion less than ~ 6 km s^{-1}. This limit is still larger than the upper limit for the proper motion in b-direction (perpendicular to the plane), which is found to be ~ 1 km s^{-1}. However, the upper limit of Sgr A*'s in-plane motion is significantly smaller than Θ_0 itself (which ranges 223–248 km s^{-1} in the present paper), indicating that Sgr A* is truly at the dynamical center of the Galactic rotation.

Miyamoto & Zhu (1998) analyzed HIPPARCOS data of OB stars and Cepheid variables, and derived $\Omega_\odot = 32.7 \pm 1.4$ km s^{-1} kpc^{-1} from the OB stars and $\Omega_\odot = 30.4 \pm 1.4$ km s^{-1} kpc^{-1} from the Cepheids, respectively. Note that here the results by Miyamoto & Zhu (1998) are converted to $\Omega_\odot$ by using their own determination of the Solar motion, which was $V_\odot \sim 15$ km s^{-1}. Our result of $\Omega_\odot$ lies in the middle of these two results and consistent with both of them. Earlier studies of Galactic parameters based on VLBI astrometry also resulted in similar values. For instance, Reid et al.(2009b) obtained Ω_0 =30.3±0.9 km s^{-1} kpc^{-1} based on $V_\odot = 5.25$ km s^{-1}, yielding $\Omega_\odot = 30.9 \pm 0.9$ km s^{-1} kpc^{-1}. Reanalysis of the same astrometry data also resulted in similar range of $\Omega_\odot$, with 30.9 to 32.5 km s^{-1} kpc^{-1} (McMillan & Binney 2010) and 32.9±1.22 km s^{-1} kpc^{-1} (Bobylev & Bajkova 2010). These results also support that $\Omega_\odot$ slightly larger than 30 km s^{-1} kpc^{-1}. On the other hand, if one adopts IAU recommendations of Galactic constants, one would obtain $\Omega_\odot$=(220+15)/8.5=27.6 km s^{-1} kpc^{-1}. Therefore, the present paper as well as recent other studies on $\Omega_\odot$ strongly suggest that the Galactic angular velocity should require an upward modification by 10% level. Because Θ_0 is tightly linked to Ω_0, the same applies to the rotation velocity of the LSR Θ_0: while the resultant values of Θ_0 are dependent of $V_\odot$ as well as R_0, our results of Θ_0 range between 223 km s^{-1} and 248 km s^{-1}, being higher than the IAU recommendation of Θ_0=220 km s^{-1}.

6.3. Source peculiar motion and $V_\odot$

As we have found in the previous section, the U and W components of the mean source peculiar motion are independent of $V_\odot$ and hence well constrained. As summarized in table 7, the mean perpendicular motion $W_{\rm src} (= -1.41 \pm 1.19$ km s^{-1}) can be regarded as 0 at 1.2-σ level, which is naturally expected from the equilibrium of Galactic disk. The U component is also 0 within the error bar, and we can safely conclude that the U component is negligible when compared to the Galactic rotation velocity, which is an order of ~ 240 km s^{-1}.

On the other hand, as we have seen in the previous section,

the V component of the source mean motion is tightly correlated with $V_\odot$, and thus exact value cannot be fixed based solely on the VLBI astrometry data. The only constraint we can obtain is the linear relation between $V_\odot$ and $V_{\rm src}$ given in equation (12). If we adopt $V_\odot = 5.25$ km s^{-1} of Dehnen & Binney (1998), then $V_{\rm src}$ becomes -14 ± 2 km s^{-1}. Therefore, our result confirms the findings by Reid et al.(2009b) that the star-forming regions lag behind the Galactic rotation. It is remarkable that this confirmation is done based on much larger number of sources compared to that in Reid et al.(2009b). However, as we have already seen, models without $V_{\rm src}$ also provide a reasonable fit to the data: χ^2 only slightly vary with changing $V_\odot$ or solving for it with assuming $V_{\rm src} = 0$ km s^{-1} (see, e.g., results 12, 15, and 18 in table 5). Therefore, at this stage we cannot conclude whether or not a Galaxy model with the rotation lag of the star-forming regions is better than a model with larger $V_\odot$ and no lag. However, the strong relation in equation [12] will provide a good base of future investigations on this problem: once one of the parameters ($V_\odot$ or $V_{\rm src}$) is determined based on other observations etc., one can immediately find the conclusion on the (non)existence of the SFRs lag.

6.4. Rotation Curve

While a few Galactic parameters still have a considerable uncertainty depending on the Solar motion etc., the shape of the rotation curve itself is well determined based on the analyses in the previous section. Figure 6 shows an example of the rotation curve, based on result 1. Here we adopted from table 3 Galactic parameters of $R_0 = 8.27$ kpc and $\Omega_0 = 29.98$ km s^{-1} kpc^{-1} (or Θ_0=248 km s^{-1}), respectively. As seen in the figure, the rotation curve can be basically regarded as "flat" between 4 kpc and 15 kpc, being consistent with the rotation curves of other galaxies with rotation velocities comparable to that of the Milky Way Galaxy (e.g., Sofue & Rubin 2001).

The flat rotation curve is also consistent with previous studies of the Galactic rotation curves (e.g., Clemens et al. 1985). On the other hand, Honma & Sofue (1997) showed that the shape of HI rotation curve is strongly dependent on Θ_0 and for a flat rotation curve, their preferred value of Θ_0 is around 200 km s^{-1}. This Θ_0 is inconsistent with the results of the VLBI astrometry here, which suggested Θ_0 much higher than the IAU standard value of 220 km s^{-1}. For solving this discrepancy, again the Solar motion would be a clue, because both of the HI rotation curve and Galaxy parameters based on VLBI astrometry are significantly affected by the Solar motion $V_\odot$.

The flatness of the rotation curve strongly constrained here can be used to estimate the distribution of dark matter in the Galaxy. In fact, in order to sustain this flat rotation curve, a considerable amount of dark matter is required. For instance, suppose that the Galaxy's disk is an exponential disk with a scale length of $h = 3$ kpc and maximum disk rotation velocity equal to Θ_0, and the mass-to-light ratio is constant through the disk. Then, as is discussed in Honma et al. (2007), the ratio of disk mass to the total mass within 13 kpc is around 0.7, and hence 30% of the total mass should be in the form of dark matter.

Note that the data points in figure 6 mostly lie below the best-fit rotation curve. This is obviously the effect of the lag of the star-forming regions because in figure 6 we adopt the Solar motion of 5.25 km s^{-1} that makes the lag largest among the results in table 5. If larger $V_\odot$ is adopted, then the lag will be reduced and the data points should scatter around the model curve. Other interesting feature in figure 6 is that the deviation of the sources from the rotation curve could be systematic (such as lower rotation velocity at Galacto-centric radii of 5 kpc and 9 kpc). Although the number of the sample sources is not enough to discuss this at the present, this may be related to non-axisymmetric structure of the Galaxy (such as a bar and spiral arms), and so this will be interesting target for future studies with more sources.

We are grateful to anonymous referee for careful reading of the manuscript and constructive suggestions. One of the authors (MH) acknowledges the financial support from grant-in-aid (No.21244019) by the Ministry of Education, Culture, Sports, Science and Technology (MEXT). The authors also thank all the staff members at Mizusawa VLBI observatory for supporting the observations.

References

Ando, K., et al. 2011, PASJ, 63, 45
Asaki, Y., Deguchi, S., Imai, H., Hachisuka, K., Miyoshi, M., & Honma, M. 2010, ApJ, 721, 267
Aumer, M., & Binney, J., 2009, MNRAS, 397, 1286
Bartkiewicz, A., Brunthaler, A., Szymczak, M., van Langevelde, H. J., & Reid, M. J. 2008, A&A, 490, 787
Bobylev V. V., & Bajkova A. T., 2010, MNRAS, 408, 1788
Brunthaler, A., Reid, M. J., Menten, K. M., Zheng, X. W., Moscadelli, L., & Xu, Y. 2009, ApJ, 693, 4 24
Clemens D. P., 1985, ApJ, 295, 422
Choi, Y. K., et al. 2008, PASJ, 60, 1007
Dame, T. M., Hartmann, D., & Thaddeus, P. 2001, ApJ, 547, 792
Dehnen, W., Binney, J., 1998, MNRAS, 298, 387
Dzib, S., Loinard, L., Mioduszewski, A. J., Boden, A. F., Rodríguez, L. F., & Torres, R. M. 2010, ApJ, 718, 610
Ghez, A. M., Salim, S., Weinberg, N. N., et al. 2008, ApJ, 689, 1044
Gillessen, S., Eisenhauer, F., Trippe, S., et al. 2009, ApJ, 692, 1075
Hachisuka, K., Brunthaler, A., Menten, K. M., Reid, M. J., Hagiwara, Y., & Mochizuki, N. 2009, ApJ, 696, 1981
Hirota, T., et al. 2008, PASJ, 60, 37
Hirota, T., et al. 2008, PASJ, 60, 961
Hirota, T., Honma, M., Imai, H., Sunada, K., Ueno, Y., Kobayashi, H., & Kawaguchi, N. 2011, PASJ, 63, 1
Honma, M., & Sofue, Y. 1997, PASJ, 49, 453
Honma, M., et al. 2007, PASJ, 59, 889
Honma, M., Hirota, T., Kan-Ya, Y., Kawaguchi, N., Kobayashi, H., Kurayama, T., & Sato, K. 2011, PASJ, 63, 17
Imai, H., et al. 2007, PASJ, 59, 1107
63, 81
Kerr, F. J., & Lynden-Bell, D. 1986, MNRAS, 221, 1023
Kim, M. K., et al. 2008, PASJ, 60, 991
Kurayama, T., Nakagawa, A., Sawada-Satoh, S., Sato, K., Honma, M., Sunada, K., Hirota, T., & Imai, H. 2011, arXiv:1102.2056
Loinard, L., Torres, R. M., Mioduszewski, A. J., Rodríguez, L. F., González-Lópezlira, R. A., Lachaume, R., Vázquez, V., & González, E. 2007, ApJ, 671, 546
Loinard, L., Torres, R. M., Mioduszewski, A. J., & Rodríguez, L. F. 2008, ApJL, 675, L29
Matsunaga, N., Kawadu, T., Nishiyama, S., Nagayama, T., Hatano, H., Tamura, M., Glass, I. S., & Nagata, T. 2009, MNRAS, 399, 1709

McMillan P. J., & Binney J. J., 2010, MNRAS, 402, 934
Miyamoto M., & Zhu Z., 1998, AJ, 115, 1483
Moellenbrock, G. A., Claussen, M. J., & Goss, W. M. 2009, ApJ, 694, 192
Moscadelli, L., Reid, M. J., Menten, K. M., Brunthaler, A., Zheng, X. W., & Xu, Y. 2009, ApJ, 693, 406
Moscadelli, L., Cesaroni, R., Rioja, M. J., Dodson, R., & Reid, M. J. 2011, A&A, 526, A66
Motogi, K., Sorai, K., Habe, A., Honma, M., Kobayashi, H., & Sato, K. 2011, PASJ, 63, 31
Nagayama, T., Omodaka, T., Nakagawa, A., Handa, T., Honma, M., Kobayashi, H., Kawaguchi, N., & Miyaji, T. 2011, PASJ, 63, 23
Nagayama, T., Omodaka, T., Nakagawa, A., Handa, T., Honma, M., Kobayashi, H., Kawaguchi, N., & Ueno, Y. 2011, arXiv:1104.0363
Niinuma, K., et al. 2011, PASJ, 63, 9
Oh, C. S., Kobayashi, H., Honma, M., Hirota, T., Sato, K., & Ueno, Y. 2010, PASJ, 62, 101
Reid, M. J. 1993, ARA&A, 31, 345
Reid, M. J., Brunthaler, A., 2004, ApJ, 616, 872
Reid, M. J., Menten, K. M., Brunthaler, A., Zheng, X. W., Moscadelli, L., & Xu, Y. 2009a, ApJ, 693, 397
Reid, M. J., Menten, K. M., Zheng, X. W., et al. 2009b, ApJ, 700, 137
Reid, M. J., Menten, K. M., Zheng, X. W., Brunthaler, A., & Xu, Y. 2009c, ApJ, 705, 1548
Rygl, K. L. J., Brunthaler, A., Reid, M. J., Menten, K. M., van Langevelde, H. J., & Xu, Y. 2010, A&A, 511, A2
Rygl, K. L. J., Brunthaler, A., Sanna, A., et al. 2012, A&A, 539, A79
Sakai, N., et al. 2012, PASJ, 64, in press
Sanna, A., Reid, M. J., Dame, T. M., et al. 2012, ApJ, 745, 82
Sanna, A., Reid, M. J., Moscadelli, L., Dame, T. M., Menten, K. M., Brunthaler, A., Zheng, X. W., & Xu, Y. 2009, ApJ, 706, 464
Sato, M., et al. 2008, PASJ, 60, 975
Sato, M., Hirota, T., Reid, M. J., Honma, M., Kobayashi, H., Iwadate, K., Miyaji, T., & Shibata, K. M. 2010, PASJ, 62, 287
Sato, M., Reid, M. J., Brunthaler, A., & Menten, K. M. 2010, ApJ, 720, 1055
Schönrich R., Binney J. J., Dehnen W., 2010, MNRAS, 403, 1829
Shiozaki, S., Imai, H., Tafoya, D., et al. 2011, PASJ, 63, 1219
Sofue Y., Rubin V., 2001, ARA&A, 39, 137
Torres, R. M., Loinard, L., Mioduszewski, A. J., & Rodríguez, L. F. 2007, ApJ, 671, 1813
Torres, R. M., Loinard, L., Mioduszewski, A. J., & Rodríguez, L. F. 2009, ApJ, 698, 242
Xu, Y., Reid, M. J., Zheng, X. W., & Menten, K. M. 2006, Science, 311, 54
Xu, Y., Reid, M. J., Menten, K. M., Brunthaler, A., Zheng, X. W., & Moscadelli, L. 2009, ApJ, 693, 413
Xu, Y., Moscadelli, L., Reid, M. J., et al. 2011, ApJ, 733, 25
Zhang, B., Zheng, X. W., Reid, M. J., Menten, K. M., Xu, Y., Moscadelli, L., & Brunthaler, A. 2009, ApJ, 693, 419

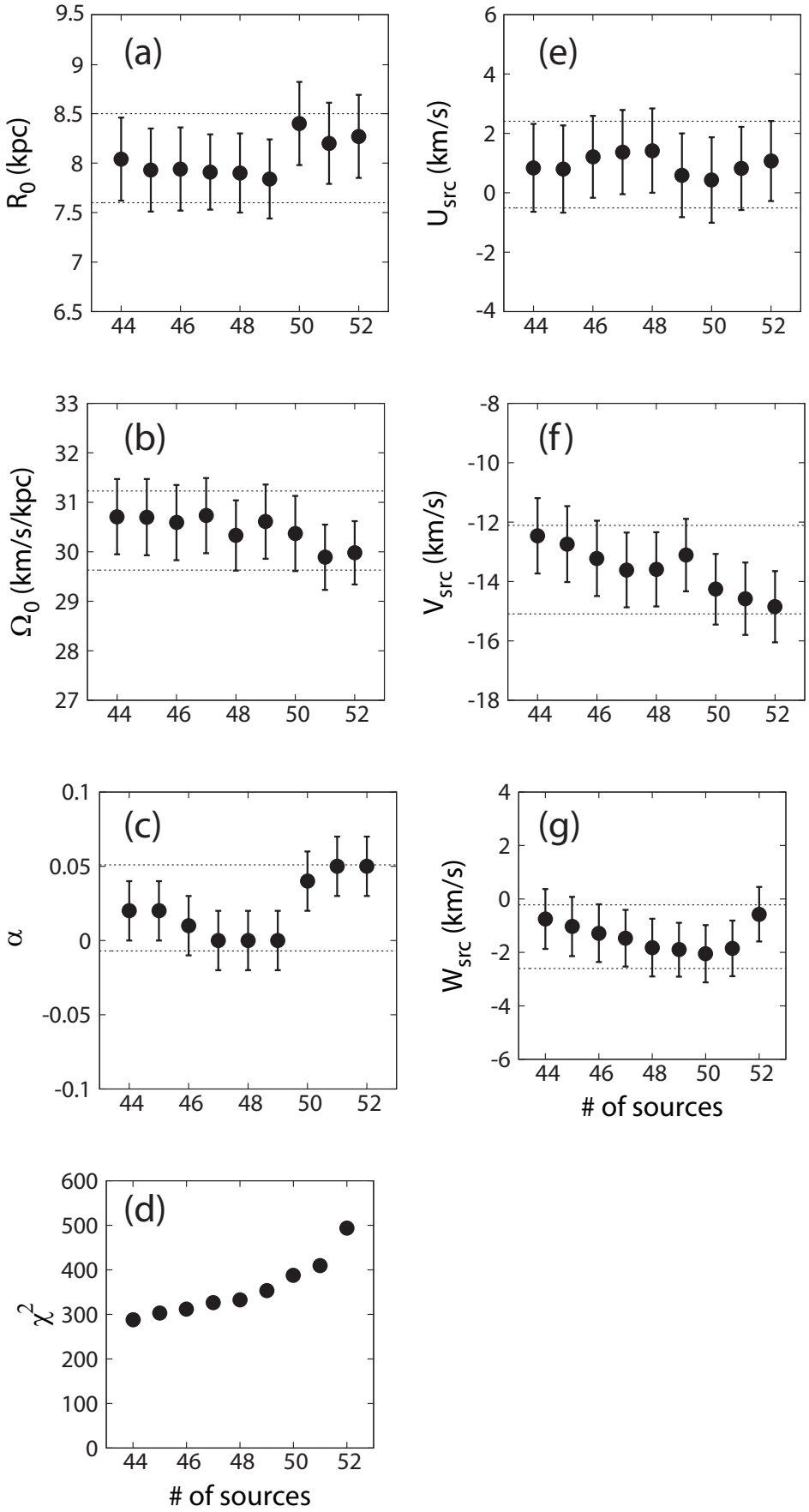

Fig. 2. Galactic parameters obtained in results 1–9 in table 3. From top left to bottom (a to d): for R_0, Ω_0, α and χ^2. From top right to bottom (e to g): for $U_{\rm src}$, $V_{\rm src}$, and $W_{\rm src}$. Error bars of each point show statistical uncertainties obtained with the MCMC analyses (1σ). All figures are plotted as a function of the number of sample sources. Dotted lines show the range of our best estimates including systematics introduced by different samples with/without possible "outliers".

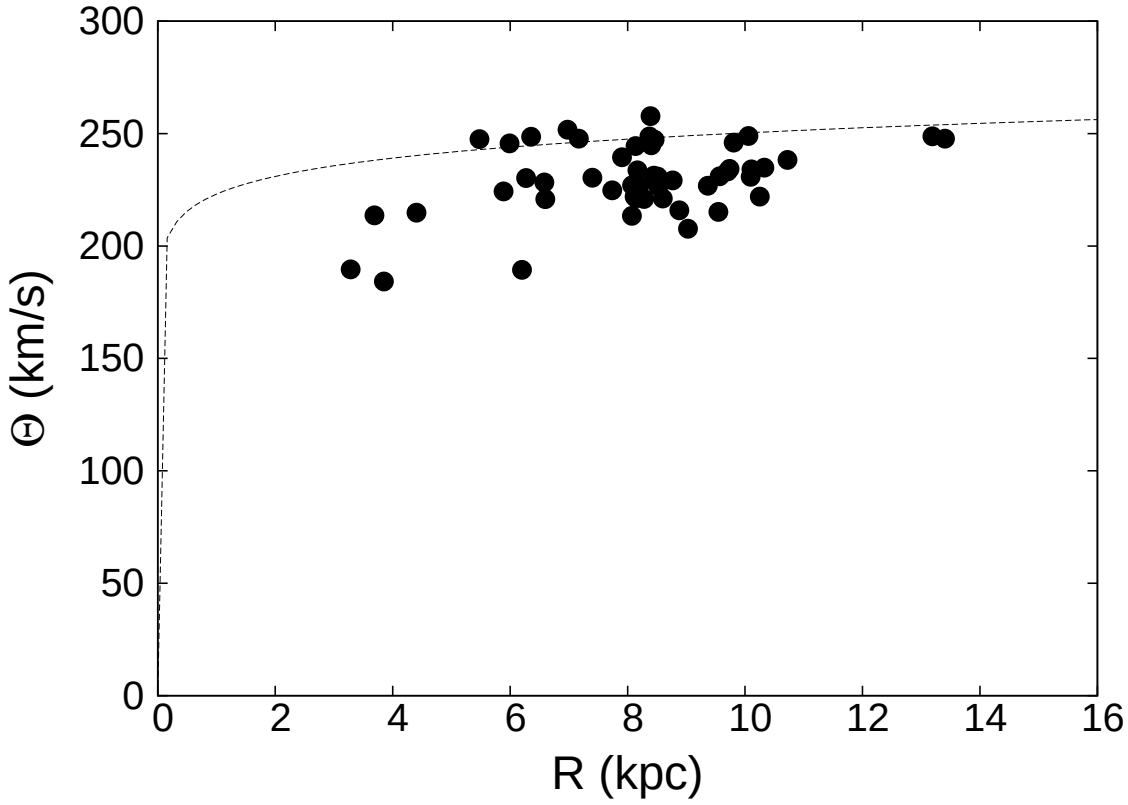

Fig. 6. Rotation curve plot for result 1 (52 sources). Filled circles correspond to the observed sources. Values of R_0 and Θ_0 are taken from the relevant results in table 1 ($R_0 = 8.27$ kpc, $\Omega_0 = 29.98$ km s^{-1} kpc^{-1} and thus $\Theta_0 = R_0 \times \Omega_0 = 248$ km s^{-1}). Here error bars are not shown because in most cases they are invisibly small in this plot (but note that the systematic effect is considerably large as described in the text). Dotted line shows a rotation curve with $\Theta_0 = 248$ km s^{-1} and a power low index $\alpha = 0.05$. Note that here $V_\odot = 5.25$ km s^{-1} is adopted and hence the lag of SFRs against Galactic rotation is prominent (by ~ 15 km s^{-1}), with most of data points located below the model rotation curve.

Table 1. Parallaxes and proper motions for 52 sources.

Source	l (deg)	b (deg)	π (mas)	$v_{\rm LSR}$ (km s^{-1})	$\mu_\alpha \cos\delta$ (mas yr^{-1})	μ_δ (mas yr^{-1})	Ref.	rank in $P_i(\mathbf{O_i}\|\mathbf{M})$
G 5.89−0.39	5.89	−0.39	0.780 ± 0.050	9 ± 3	0.17 ± 0.42	-0.95 ± 0.34	19	
G 9.62+0.20	9.62	0.20	0.194 ± 0.023	2 ± 5	-0.58 ± 0.05	-2.49 ± 0.27	28	3
G 12.89+0.49	12.89	0.49	0.428 ± 0.022	40 ± 3	0.16 ± 0.03	-1.90 ± 1.59	38	
G 14.33−0.64	14.33	−0.64	0.893 ± 0.101	22 ± 10	0.95 ± 2.00	-2.50 ± 2.00	31	
G 15.03−0.68	15.03	−0.68	0.505 ± 0.033	23 ± 3	0.68 ± 0.05	-1.42 ± 0.09	38	
G 23.01−0.41	23.01	−0.41	0.218 ± 0.017	82 ± 3	-1.72 ± 0.04	-4.12 ± 0.30	4	
G 23.44−0.18	23.44	−0.18	0.170 ± 0.032	98 ± 3	-1.93 ± 0.10	-4.11 ± 0.07	4	
G 23.66−0.13	23.66	−0.13	0.313 ± 0.039	83 ± 2	-1.32 ± 0.02	-2.96 ± 0.03	3	
G 27.36−0.16	27.36	−0.16	0.125 ± 0.042	92 ± 3	-1.81 ± 0.08	-4.11 ± 0.26	38	
EC 95 (Serpens)	31.56	5.33	2.410 ± 0.020	9 ± 3	0.70 ± 0.02	-3.64 ± 0.10	6	
G 35.20−0.74	35.20	−0.74	0.456 ± 0.045	28 ± 3	-0.18 ± 0.06	-3.63 ± 0.11	39	
G 35.20−1.74	35.20	−1.74	0.306 ± 0.045	42 ± 3	-0.71 ± 0.05	-3.61 ± 0.17	39	
G 48.61+0.02	48.61	0.02	0.199 ± 0.007	19 ± 1	-2.76 ± 0.04	-5.28 ± 0.11	21	2
W 51 Main/South	49.48	−0.39	0.185 ± 0.010	58 ± 4	-2.64 ± 0.16	-5.11 ± 0.16	32	
IRAS 19213+1723	52.10	1.04	0.251 ± 0.036	42 ± 3	-2.53 ± 0.05	-6.07 ± 0.06	23	
G 59.78+0.06	59.78	0.06	0.463 ± 0.020	27 ± 3	-1.65 ± 0.03	-5.12 ± 0.08	37	
ON1	69.54	−0.98	0.404 ± 0.017	12 ± 1	-3.10 ± 0.18	-4.70 ± 0.24	20	
G 75.30+1.32	75.30	1.32	0.108 ± 0.005	-57 ± 2	-2.37 ± 0.09	-4.48 ± 0.17	29	
ON2N	75.78	0.34	0.261 ± 0.009	0 ± 1	-2.79 ± 0.13	-4.66 ± 0.17	1	
IRAS 20126+4104	78.12	3.64	0.610 ± 0.020	-4 ± 3	-10.25 ± 0.02	-2.30 ± 0.28	18	1
AFGL 2591	78.89	0.71	0.300 ± 0.010	-6 ± 3	-1.20 ± 0.32	-4.80 ± 0.12	26	5
IRAS 20290+4052	79.74	0.99	0.737 ± 0.062	-1 ± 3	-2.84 ± 0.09	-4.14 ± 0.54	26	
DR 20	80.86	0.38	0.687 ± 0.038	-3 ± 3	-3.29 ± 0.13	-4.83 ± 0.26	26	
DR 21	81.75	0.59	0.666 ± 0.035	-3 ± 3	-2.84 ± 0.15	-3.80 ± 0.22	26	
W 75 N	81.87	0.78	0.772 ± 0.042	9 ± 3	-1.97 ± 0.10	-4.16 ± 0.15	26	
AFGL 2789	94.60	−1.80	0.326 ± 0.031	-44 ± 3	-2.20 ± 0.08	-3.77 ± 0.15	23	8
IRAS 22198+6336	107.29	5.64	1.309 ± 0.047	-11 ± 3	-2.47 ± 0.21	0.26 ± 0.40	9	
L 1206	108.18	5.52	1.289 ± 0.153	-12 ± 3	0.27 ± 0.23	-1.40 ± 1.95	25	
Cep A HW 2	109.87	2.11	1.430 ± 0.080	-10 ± 5	0.50 ± 1.10	-3.70 ± 0.20	17	
NGC 7538	111.54	0.78	0.378 ± 0.017	-57 ± 3	-2.45 ± 0.03	-2.44 ± 0.06	17	6
L 1287	121.29	0.66	1.077 ± 0.039	-24 ± 3	-0.86 ± 0.11	-2.29 ± 0.56	25	
IRAS 00420+5530	122.02	−7.07	0.460 ± 0.010	-46 ± 3	-2.52 ± 0.05	-0.84 ± 0.05	16	
NGC 281	123.07	−6.31	0.355 ± 0.030	-31 ± 3	-2.63 ± 0.05	-1.86 ± 0.08	30	
W 3 OH	133.95	1.06	0.512 ± 0.010	-45 ± 3	-1.20 ± 0.20	-0.15 ± 0.20	36	
S Per	134.62	−2.20	0.413 ± 0.017	-39 ± 3	-0.49 ± 0.23	-1.19 ± 0.20	2	
WB 89-437	135.28	2.80	0.167 ± 0.006	-72 ± 2	-1.22 ± 0.30	0.46 ± 0.36	7	
L 1448 C	157.57	−21.94	4.310 ± 0.330	5 ± 3	21.90 ± 0.70	-23.10 ± 3.30	10	
NGC 1333	158.29	−20.50	4.250 ± 0.320	8 ± 3	14.25 ± 2.58	-8.95 ± 0.74	8	
Hubble 4 (Taurus)	168.84	−15.52	7.530 ± 0.030	15 ± 2	4.30 ± 0.05	-28.90 ± 0.30	34	
IRAS 05168+3634	170.66	−0.25	0.532 ± 0.053	-16 ± 2	0.23 ± 1.07	-3.14 ± 0.28	27	
HP-Tau/G2 (Taurus)	175.73	−16.24	6.200 ± 0.030	18 ± 2	13.85 ± 0.03	-15.40 ± 0.20	35	
T-Tau/Sb (Taurus)	176.23	−20.89	6.820 ± 0.030	19 ± 1	4.02 ± 0.03	-1.18 ± 0.05	15	4
IRAS 06061+2151	188.79	1.03	0.496 ± 0.031	-2 ± 1	-0.10 ± 0.10	-3.91 ± 0.07	22	7
S 252/IRAS 06058+2138	188.95	0.89	0.476 ± 0.006	11 ± 3	0.02 ± 0.01	-2.02 ± 0.04	24	
G 192.16−3.84	192.16	−3.84	0.660 ± 0.040	6 ± 3	0.84 ± 0.16	-2.22 ± 0.23	33	
S 255	192.60	−0.05	0.628 ± 0.027	5 ± 1	-0.14 ± 0.54	-0.84 ± 1.76	25	
S 269	196.45	−1.68	0.189 ± 0.008	20 ± 5	-0.42 ± 0.01	-0.12 ± 0.04	11	
Orion KL	209.01	−19.38	2.390 ± 0.030	10 ± 5	9.56 ± 0.10	-3.83 ± 0.15	13	
G 232.6+1.0	232.62	1.00	0.596 ± 0.035	23 ± 3	-2.17 ± 0.06	2.09 ± 0.46	24	
VY CMa	239.35	−5.06	0.880 ± 0.080	18 ± 3	-2.09 ± 0.16	1.02 ± 0.61	5	
S1 (Ophiuchus)	353.10	16.89	8.550 ± 0.500	3 ± 3	-3.88 ± 0.87	-31.55 ± 0.69	15	
ρ Oph East	353.94	15.84	5.600 ± 1.500	3 ± 3	-20.60 ± 0.70	-32.40 ± 2.00	12	

(1) Ando et al. 2011 (2) Asaki et al. 2010 (3) Bartkiewicz et al. 2008 (4) Brunthaler et al. 2009 (5) Choi et al. 2008
(6) Dzib et al. 2010 (7) Hachisuka et al. 2009 (8) Hirota et al. 2008a (9) Hirota et al. 2008b (10) Hirota et al. 2011
(11) Honma et al. 2007 (12) Imai et al. 2007 (13) Kim et al. 2008 (14) Loinard et al. 2007 (15) Loinard et al. 2008
(16) Moellenbrock et al. 2009 (17) Moscadelli et al. 2009 (18) Moscadelli et al. 2011 (19) Motogi et al. 2011 (20) Nagayama et al. 2011a
(21) Nagayama et al. 2011b (22) Niinuma et al. 2011 (23) Oh et al. 2010 (24) Reid et al. 2009a (25) Rygl et al. 2010 (26) Rygl et al. 2012 (27) Sakai et al. 2011 (28) Sanna et al. 2009 (29) Sanna et al. 2012 (30) Sato et al. 2008 (31) Sato et al. 2010a (32) Sato et al. 2010b (33) Shiozaki et al. 2011 (34) Torres et al. 2007 (35) Torres et al. 2009 (36) Xu et al. 2006 (37) Xu et al. 2009 (38) Xu et al. 2011 (39) Zhang et al. 2009